Climate Dynamics (2025) 63:247
https://doi.org/10.1007/s00382-025-07725-5

ORIGINAL ARTICLE

Spatial patterns and drivers of elevation dependency of extreme temperature changes on the Tibetan Plateau

Ke Yang[1] · **Weizhe Chen**[1] · **Guoyu Ren**[2,3] · **Rui Zhang**[4]

Received: 11 November 2024 / Accepted: 28 April 2025 / Published online: 6 June 2025

Abstract
The Tibetan Plateau (TP) has experienced rapid warming and a series of extreme climate events in recent decades, severely impacting ecosystems of local and downstream areas. The stratification of temperature change with elevation is particularly pronounced on TP. However, understanding of the spatial heterogeneity of elevation-dependent extreme temperature change remains limited due to unevenly distributed meteorological stations. This paper first obtains the spatial elevation-dependent pattern of extreme temperature change by applying a moving window model to daily gridded air temperature data from 1979 to 2018, and quantifies the specific contribution of underlying physical mechanisms based on GeoDetector model. The results show that there are four types of elevation-dependent patterns, including warming trends that strengthen/weaken with elevation (EDW+/-) and cooling trends that strengthen/weaken with elevation (EDC+/-). EDW+is concentrated in southeastern TP and EDW- is in northern and central TP. EDC+mainly occurs in northeastern TP and EDC- is in northern Inner TP. The total cloud cover is the main cause of elevation amplification effect of extreme temperature change (i.e., EDW+and EDC+) through regulating the absorption of shortwave radiation at different elevations. Snow cover is the main cause of elevation diminution effect (i.e., EDW- and EDC-) through influencing surface albedo. This paper reveals the distribution and causes of elevation-dependent patterns, providing new insights into alpine environmental change.

Keywords Extreme temperature · Elevation dependency · Spatial patterns · Physical mechanisms · Tibetan Plateau

1 Introduction

The Tibetan Plateau (TP) (Fig. 1a) is the largest and highest plateau on Earth with an average elevation of more than 4000 m above sea level (Qin et al. 2020; Yang et al. 2014). It has the largest cryosphere (i.e., snow, glacier, and permafrost) of freshwater resources outside the polar regions and thus becomes the birthplace of the great rivers of Asia, such as the Yangtze River, the Yellow River, the Brahmaputra River (Kang et al. 2019; Yao et al. 2019; Yan et al. 2020). Its unique topography and landscape make it one of the most climatically sensitive and ecologically fragile regions in the world (Yao et al. 2012; Kuttippurath et al. 2024). TP profoundly impacts the climate and natural ecosystems far beyond the plateau itself.

Over the past decades, TP has experienced rapid warming, with increasingly frequent and intense warm extreme events and a decline in cold extreme events (Chen and Sun 2015; Sun et al. 2017; Guo et al. 2019; Huang et al. 2023; Rangwala and Miller 2012; You et al. 2008), leading to glacier retreat and shrinkage (Yang et al. 2019), permafrost degradation (Mu et al. 2020), spring vegetation phenology advancement (Post et al. 2018), ecological systems change (Zhu et al. 2023) and an increase in natural disasters such as landslides and glacial lake outburst floods (Liu et al. 2021; Tang et al. 2023). This has raised concerns about the patterns

✉ Weizhe Chen
wzchen@cug.edu.cn

1 School of Earth Sciences, Hubei Key Laboratory of Critical Zone Evolution, China University of Geosciences, Wuhan, China

2 Department of Atmospheric Science, School of Environmental Science, China University of Geosciences, Wuhan, China

3 Laboratory for Climate Studies, National Climate Center, China Meteorological Administration (CMA), Beijing, China

4 College of Urban and Environmental Sciences, Hubei Normal University, Huangshi, China

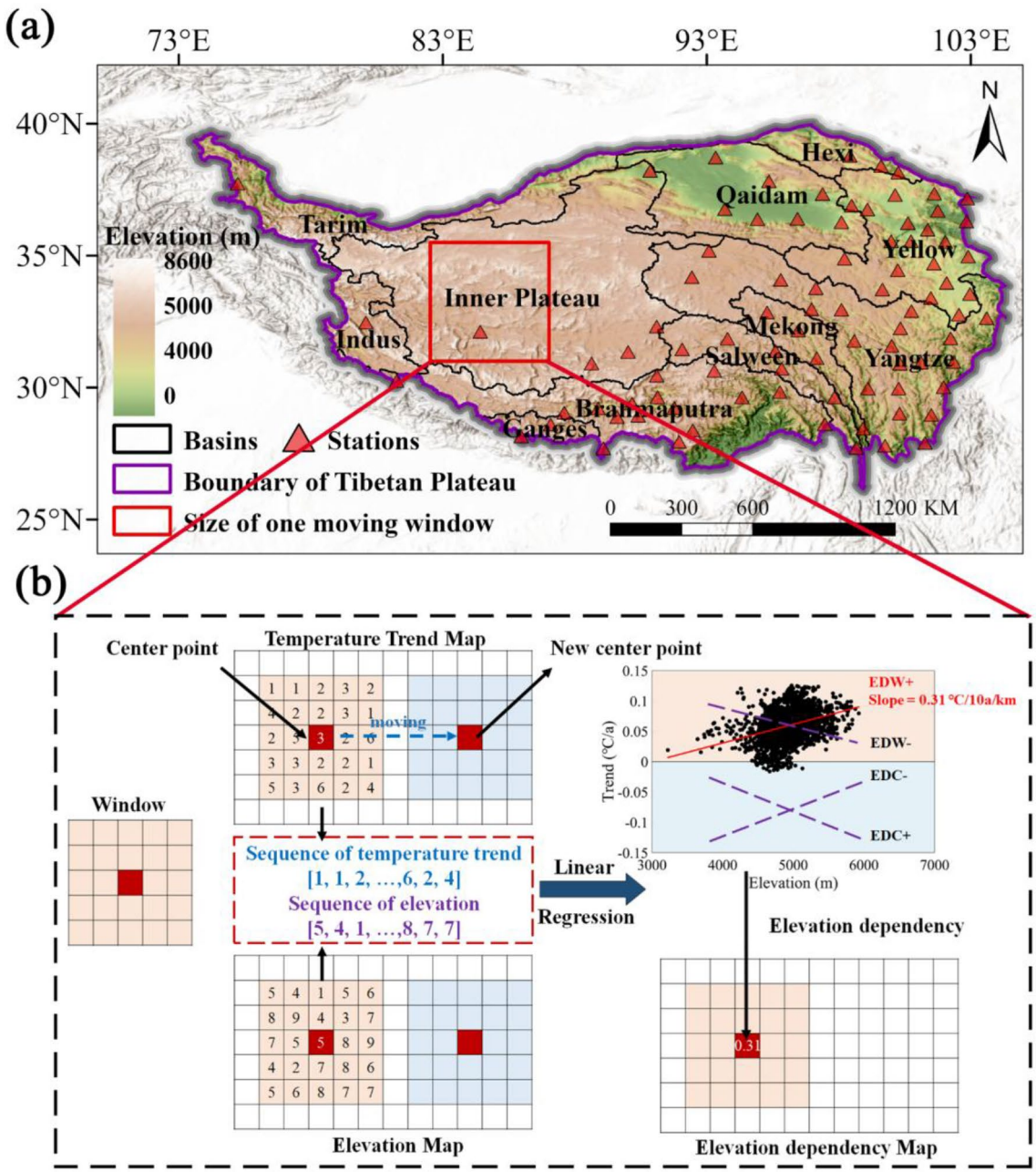

Fig. 1 Location of the study area and the schematic of the moving window model. (**a**) is the topographic map and the location of 12 basins of the Tibetan Plateau. (**b**) illustrates the operation of the moving window. The numbers in the temperature trend and elevation maps are not actual values, they are only used for demonstration purposes. The graph in the upper right corner represents linear regression between elevation and temperature trend in one moving windows. The slope indicates elevation dependency. The graphs also illustrate four different patterns of elevation dependency, including EDW+/-, and EDC+/-. With increasing elevation, a faster/slower increase in temperature trend is classified as EDW+/-, while a larger/smaller decrease in temperature trend is classified as EDC+/-. The solid lines represent the actual regression results, while the dashed lines are for illustration only

of temperature change on the TP. Notably, a phenomenon known as elevation-dependent warming (EDW) is particularly pronounced on the TP. It refers to the stratification of temperature change with elevation, often with faster warming rate in high-elevation areas compared to low-elevation areas(Liu et al. 2009; Pepin et al. 2015; You et al. 2020a, b; Toledo et al. 2022). One of the pioneer studies using 165 in situ observations reveals a clear EDW phenomenon (Liu and Ping 1998), and subsequent studies have continued to demonstrate the existence of the phenomenon (Liu and Chen 2000; Pepin et al. 2015; Wei and Fang 2013; Ahamed et al. 2024). Since extreme climate events are more sensitive

to global warming than the average climate state and can make more severe impacts on ecosystems (Ha and Yun 2012; Schoetter et al. 2015; Lewis et al. 2017), it is critical to understand the relationship between climate extremes and elevation in high mountain regions.

Although there is a strong consensus on the pattern of temperature change on the TP, insignificant EDW has been observed in some cases and even negative EDW (warming rate decreasing with elevation) has been reported (Lu et al. 2010; Guo and Wang 2012; Cuo et al. 2013; Du et al. 2019). The argument is attributed to the sparse and uneven distribution of meteorological stations on the plateau, making it challenging to fully capture the patterns of temperature change over the whole region. Furthermore, due to the vast expanse of the TP, elevation-dependent patterns vary across different areas. For instance, there are differences in EDW between the northern part of the TP and the southern and eastern regions (Li et al. 2020; Pepin et al. 2022). However, most studies have overlooked the spatial heterogeneity of the EDW. Reanalysis data and remote sensing data provide a new way to monitor the pattern of warming. They have the advantages of wide coverage, spatial continuity and high resolution, and have been widely used in EDW research (Guo et al. 2019; Pepin et al. 2019; You et al. 2010; Zou et al. 2014).

Recent studies reveal the importance of the physical mechanisms to explain EDW phenomenon (Dimri et al. 2022). The snow/ice albedo feedback is the most common mechanism. Snow cover reduces surface temperatures by decreasing the absorption of solar radiation (Zhang et al. 2022). The most pronounced warming occurs in regions where the snowline is retreating, particularly near the 0 °C isotherm. As the snowline shifts upward, the warming effect extends to higher elevations, intensifying temperature increases in these areas (Kang et al. 2010; Ghatak et al. 2014; Rangwala et al. 2016; Che et al. 2019). The atmospheric vapor feedback is also a potentially important contributor to EDW. The increase in specific humidity leads to an increase in surface downwelling longwave radiation and subsequently larger warming rate. This feedback is particularly sensitive in high-elevation regions, further amplifying elevation-dependent warming. (Pepin et al. 2015; Rangwala and Miller 2012). For the cloud feedback, cloud cover affects both shortwave and longwave radiation and thus influences the surface energy budget. Reduced daytime cloud cover at high elevations increases solar radiation absorption, accelerating warming. Conversely, increased nighttime cloud cover at high elevations enhances downward longwave radiation, raising minimum temperatures (Pepin et al. 2015; Duan and Wu 2006; Hua et al. 2018). Furthermore, some studies point out that vegetation may have an influence on EDW over the TP. A general greening of vegetation across the TP has been observed, accompanied by a decrease in albedo and an increase in evapotranspiration. The cooling effect driven by evapotranspiration is dominant on TP (Shen et al. 2015), meaning that an increase in vegetation leads to a reduction in temperature. Additionally, the growth of vegetation exhibits a negative elevation dependency (Liu et al. 2019), contributing to the formation of the EDW phenomenon (You et al. 2020a, b).

Overall, above feedback mechanisms can theoretically influence the heat flux reaching the Earth's surface directly or indirectly, leading to different temperature changes along the elevation. In fact, there are significant spatial differences in the effects of different factors on temperature changes (Li et al. 2018; Duan et al. 2015). However, most analyses consider the plateau as a whole and overlook the spatial heterogeneity of driver effects. In addition, previous studies mainly rely on simple linear relationships to examine how factors influence EDW (Guo et al. 2019; Gao et al. 2021) and fail to quantify the specific contribution of each driving factor. Therefore, the aim of this study is first to reveal the spatial patterns of elevation-dependent change in extreme temperatures by a moving window model on the TP during 1979–2018. And then we quantify the contribution of each driving factor to the pattern of extreme temperature change in different regions of TP based on the Geodetector model.

2 Methods

2.1 Data

In this paper, we use the daily gridded air temperature data, including T_{max}, T_{min}, and T_{mean}, with a spatial resolution of 0.1°×0.1° from 1979 to 2018 (Fang et al. 2022). This dataset combines multiple data sources, such as in situ data, reanalysis data, and remote sensing data. It establishes a reliable and robust air temperature model to estimate T_{max}, T_{min} and T_{mean} under different weather conditions, and employs correction equations for different regions to enhance the data accuracy. The Pearson coefficient (R^2) ranges from 0.95 to 0.99, the mean absolute error (MAE) varies from 0.47 to 1.61 °C, and the root mean square error (RMSE) ranges from 0.70 to 3.01 °C on the TP (Fang et al. 2022). Thus, the high accuracy and spatial resolution make the dataset suitable for climate change research.

The modulation of shortwave and longwave radiation influences the surface energy balance, resulting in temperature change (Kjaersgaard et al. 2009). Driving factors that affect shortwave and longwave radiation are selected, including snow cover, total cloud cover, specific humidity, and normalized difference vegetation index (NDVI). The total cloud cover data and snow cover data covering the

period between 1979 and 2018 are from the ERA5/ERA5-Land product. The ERA5/ERA5-Land dataset, published by the European Centre for Medium-Range Weather Forecasts (ECMWF), offers a spatial resolution of 0.25°/0.1° and has been proven to perform better over the TP than other reanalysis products (Mazhar et al. 2021). The specific humidity data from 1979 to 2018 is derived from the China Meteorological Forcing Dataset (He et al. 2020). It has a temporal resolution of daily scale and a spatial resolution of 0.1° × 0.1°. The NDVI data between 1982 and 2018 is from PKU GIMMS-NDVI product with a spatial resolution of 1/12° (Li et al. 2023). In this study, we resample all the influencing factor data to the resolution of 0.1°.

2.2 Methods

2.2.1 Extreme temperature indices

T_{mean}, T_{max}, T_{min} along with eight extreme temperature indices (Fig. S2) are calculated in this paper (Table 1), which are recommended by the World Meteorological Organization Expert Team on Climate Change Detection and Indices (ETCCDI) (available at http://etccdi.pacificclimate.org/index.shtml). 10th and 90th percentiles are defined relative to the base period 1981–2010. The extreme temperature indices are divided into two groups, representing the intensity (TXx, TNx, TXn, Tnn) and frequency (TX90p, TN90p, TX10p, TN10p) of extreme events, respectively. The TXx, TNx, TX90p, TN90p belong to warm events, and the remaining indices belong to cold events.

2.2.2 Linear regression analysis

The linear regression method (Yuan et al. 2021) is used at each grid point to calculate the trends of different temperature indices from 1979 to 2018 and the elevation dependency in a moving window (introduced in Sect. 2.2.3). The specific equation is shown below:

$$Slope = \frac{n \times \sum_{i=1}^{n} (i \times x_i) - \sum_{i=1}^{n} i \times \sum_{i=1}^{n} x_i}{n \times \sum_{i=1}^{n} i^2 - \left(\sum_{i=1}^{n} i\right)^2} \quad (1)$$

where $Slope$ is the change rate over the series, x_i is the value of i, and n is the total number of the series. $Slope > 0$ indicates an increasing trend while $Slope < 0$ indicates a decreasing trend. The significance of the trend is analyzed using the F-test. The calculation formula is as follows:

$$F = \frac{(n-2) \times \sum_{i=1}^{n} (\hat{x}_i - \overline{x})^2}{\sum_{i=1}^{n} (x_i - \hat{x}_i)^2} \quad (2)$$

where $\hat{x}_i$ is the regression value of the variable in i and $\overline{x}$ is the average value of variable for a given series.

2.2.3 Moving window model

The TP covers a vast area across multiple latitude zones and the temperature changes in spatially heterogeneity. Typically, the warming in high latitudes is faster than that in low latitudes (Wang et al. 2022). The influence of latitude can either offset or amplify the effect of elevation on temperature changes, thus interfering elevation dependency identification (Wu et al. 2023). Therefore, it is necessary to remove the influence of latitude and focus on the localized temperature change. To address this issue, we perform a moving window model aimed at analyzing the accurate spatial characteristics of elevation dependency of the extreme temperature. The basic idea of the moving window model is to move a fixed window over the image and perform data analysis separately on the grid points within each window. First, the size of the moving window is determined. Since different window sizes may result in varying elevation dependency,

Table 1 Description of the eleven temperature indices. The unit "d" represents "day"

Label	Name	Definition	Type	Unit
T_{mean}	Mean temperature	Mean air temperature		°C
T_{max}	Maximum temperature	Maximum air temperature		°C
T_{min}	Minimum temperature	Minimum air temperature		°C
TXx	Annual maxima of daily maximum temperature	Annual maxima value of daily maximum temperature	Intensity	°C
TNx	Annual maxima of daily minimum temperature	Annual maxima value of daily minimum temperature		°C
TXn	Annual minima of daily maximum temperature	Annual minima value of daily maximum temperature		°C
TNn	Annual minima of daily minimum temperature	Annual minima value of daily minimum temperature		°C
TX90p	Warm days	Annual count of days when daily maximum temperature > 90th percentile	Frequency	d
TN90p	Warm nights	Annual count of days when daily minimum temperature > 90th percentile		d
TX10p	Cold days	Annual count of days when daily maximum temperature < 10th percentile		d
TN10p	Cold nights	Annual count of days when daily minimum temperature < 10th percentile		d

window sizes of 2.5°, 3.5°, 4.5°, and 5.5° for T_{max}, T_{mean} and T_{min} are tested to identify the most appropriate dimensions. Then taking the first grid point of the image as the window center, the values of grid points within the window representing the temperature trend are taken as one sequence, and the values of elevation at the corresponding location is taken as another sequence. A linear regression is performed on the two sequences and the resulting gradient value is assigned to the center grid point. For windows near the TP boundary, temperature data outside China is unavailable due to data limitations. Therefore, in these windows, the analysis focuses on the relationship between temperature and elevation within the TP. Finally, the window center is moved with a step size of one grid point, while every grid point within the TP has been analyzed as a center point (Fig. 1b). The advantage of the moving window model is that it not only eliminates the influence of latitude but also captures the spatial heterogeneity of elevation dependency.

2.2.4 GeoDetector model

The GeoDetector is a statistical method for detecting the spatial heterogeneity of variables and revealing the contribution and significance of driving factors (Wang et al. 2016). This model is based on the theory that if an independent variable drives the development of a dependent variable, then the spatial patterns of these two variables should be similar. It is widely applied in the analysis of driving factors of climate change, such as warming (Wang et al. 2021), droughts (Ji et al. 2022) and snow melting (Li et al. 2022). In this study, we utilize the factor detection tool to analyze the driving factors of temperature change on TP. It can detect the spatial heterogeneity of the pattern in temperature change and quantify the contribution of different driving factors. The contribution is determined by the q-value, ranging from 0 to 1, and a larger value indicates a larger contribution of driving factors. The formula is as follows:

$$q = 1 - \frac{\sum_{h=1}^{L} N_h \sigma^2}{N\sigma^2} = 1 - \frac{SSW}{SST} \tag{3}$$

$$SSW = \sum_{h=1}^{L} N_h \sigma_h^2 \tag{4}$$

$$SST = N\sigma^2 \tag{5}$$

where $h = 1, 2, \ldots, L$ is the number of categories of variable Y or factor X; N_h and N represent the number of stratum h and the whole area, respectively; and σ_h^2 and σ^2 are the variances of stratum h and the whole area, respectively. SSW and SST are the sum of variance within stratum and the total variance of the whole area, respectively.

In this study, we combine the moving window model and the GeoDetector model to obtain the spatial map of the contribution q of driving factors. Specifically, we calculate the q-value of four driving factors in each 4.5°×4.5° moving window area and assign the q-value to the center grid point. Using the moving window to scan every grid point of TP, we can get the final contribution map of each driving factor.

3 Results

3.1 Changes in temperature extremes

All the temperature indices show that the east-central part of the TP has experienced warming in the past 40 years, and cooling in the northwestern part (Fig. 2). The average trends of T_{max}, T_{min} and T_{mean} are 0.29 °C/10a, 0.31 °C/10a and 0.12 °C/10a, respectively (where "10a" represents "decade"). The warming rate of T_{min} is greater than that of T_{max}, causing the diurnal temperature range (DTR) on the TP to decrease. For warm extremes, the intensity or frequency in most regions show a significant increasing trend, with the average rate of TXx, TNx, TX90p, and TN90p being 0.09 °C/10a, 0.31 °C/10a, 7.6 d/10a, and 9.5 d/10a, respectively. The warm extremes at night (TNx and TN90p) are more intense or frequent than during the daytime (TXx and TX90p). For the cold extremes, the trend of TNn is 0.11 °C/10a and TXn is 0.40 °C/10a, indicating a decrease of the intensity. The magnitude of the increasing trend in TXn is the largest among these temperature indices, suggesting a significant rise in daytime extreme minimum temperature on TP. The changes of TX10p and TN10p are −3.3 d/10a and −4.4 d/10a, respectively, showing a decrease in the frequency of cold events on TP (Fig. 2).

3.2 Elevation dependency of trends in temperature extreme

To determine the optimal moving window size, we evaluate the impact of various window dimensions on elevation dependency and temperature change patterns. Fig. S1 shows that the results calculated using different window sizes are spatially similar. The 4.5° window covers a slightly larger area with significant elevation-dependent temperature changes and offers higher computational efficiency. Therefore, the 4.5° window is ultimately chosen to calculate the elevation dependency of the temperature trend at each grid point. The sign and the strength of EDW is identified by the slope of the linear regression between temperature change rates and elevation. A positive slope means warming rates increase with elevation (positive EDW), while a negative slope means warming rates decrease with elevation

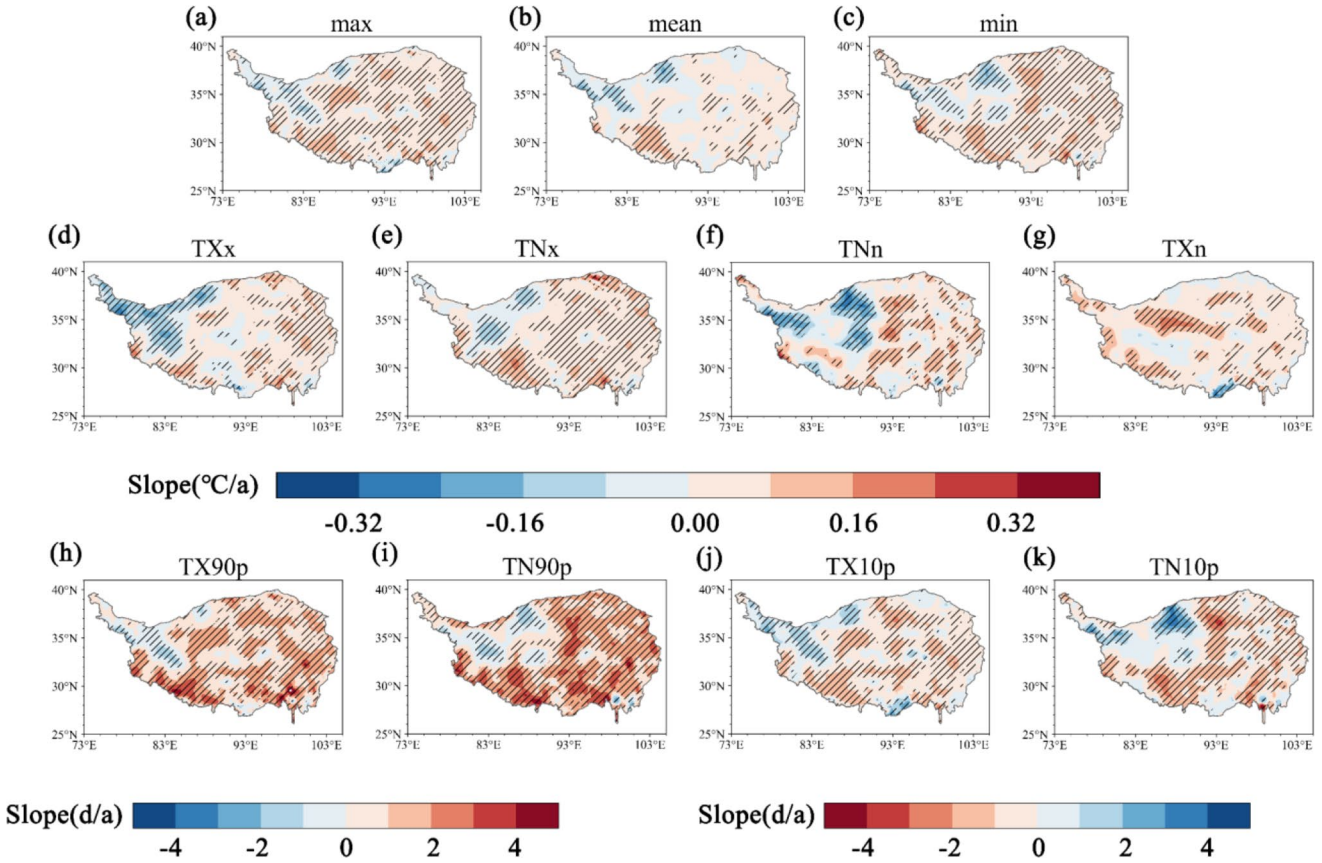

Fig. 2 Spatial trends of different temperature indices on TP from 1979 to 2018. The shaded areas indicate correlations that are significant at the 0.05 level. (**d**) - (**g**) Extreme value indices representing the intensity of temperature extremes. (**d**) and (**e**) are the warm events and (**f**) and (**g**) are the cold events. (**h**) - (**k**) Threshold indices representing the frequency of extreme events. (**h**) and (**i**) are the warm events and (**j**) and (**k**) are the cold events

(negative EDW). The positive EDW mainly occurs in the Brahmaputra River basin, the northern and southern of the Inner Tibetan Plateau, the southern of the Yellow River Basin, and the southeast of the Yangtze River basin, and the negative EDW occurs in other regions (Fig. 3a-i). Since TX10p and TN10p represent the frequency of cold events, the negative values in Fig. 3j-k indicate the positive EDW, while the positive values indicate negative EDW. This spatial pattern is opposite of the TX90p and TN90p, which represent the frequency of warm events.

Considering both temperature trends and elevation dependency, we further subdivide the EDW patterns into four categories. Positive EDW is divided into EDW+ (warming trends that become stronger with elevation) and EDC- (cooling trends that become weaker with elevation), while negative EDW is divided into EDW- (warming trends that become weaker with elevation) and EDC+ (cooling trends that become stronger with elevation) (Fig. 1b). Given the limited area of cooling regions on the TP, the stable occurrence of elevation-dependent cooling (EDC) is also relatively low with an area of 15% and concentrated in the northwestern TP (Fig. 3n). For all temperature indices, EDC+ mainly occurs in high-altitude regions above 6000 m (Fig. 4c). For T_{max}, TXx, TXn and TX10p, EDC- occurs in low-altitude regions below 2000 m, while for other indices, EDC- primarily occurs in 4500–5500 m (Fig. 4d). On the contrary, TP has experienced widespread elevation-dependent warming (EDW) over the last 40 years. For most of the extreme indices (except TXn), EDW- is the dominant pattern of temperature changes with the average area percentage of 46.60% for 10 indices, occurring primarily in the Indus basin and northern and central parts of the TP (Fig. 3n) at the elevation of 2500–5000 m (Fig. 4b). Whereas for the mean state of temperature (T_{mean}), TP is dominated by the EDW+ phenomenon with an area percentage of 40% (Fig. 3o). The robust EDW+ signal is concentrated in the southeastern part of the TP, specifically in the southern and eastern parts of the Brahmaputra River basin, the southern of the Inner Tibetan Plateau, the southern part of the Yellow River Basin, and the southeastern part of the Yangtze River basin (Fig. 3n). Besides these regions, EDW+ phenomena are also observed in the northern of the Inner TP during the daytime (Fig. 3l), the eastern part of the Yellow River Basin, the central part of the Brahmaputra River Basin,

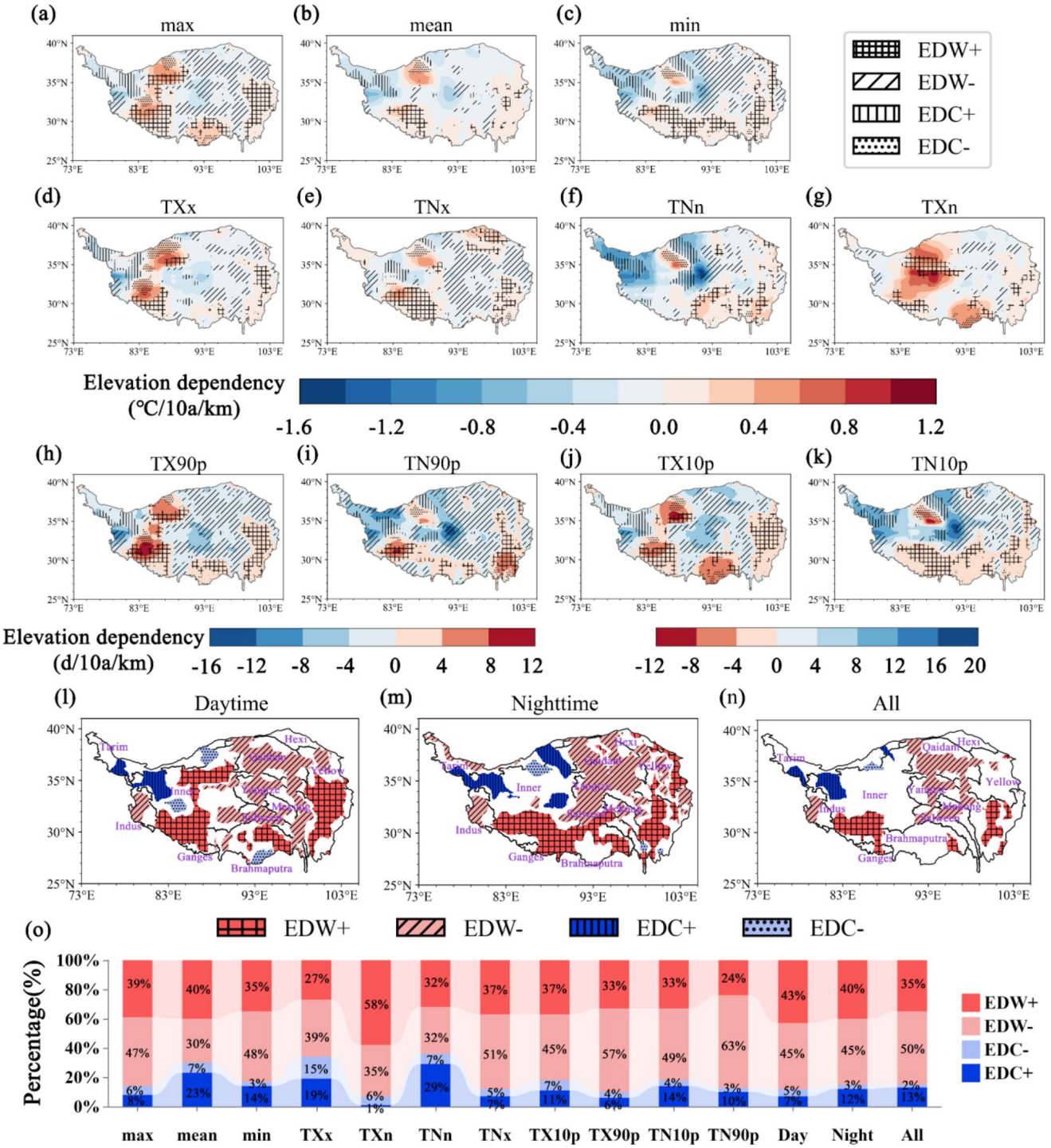

Fig. 3 Elevation dependency of different extreme temperature indices. For the four types (i.e., EDW+, EDW-, EDC+and, EDC-), only areas where elevation dependency is significant at the 0.05 level are labeled. (**l**) – (**n**) are regions where EDW+/- and EDC+/- occur centrally (EDW+/- and EDC+/- occur for more than half of the temperature indices). (**l**) is the temperature indices representing the daytime extreme events. (**m**) is that representing the nighttime extreme events, and (**n**) is all indices. (**o**) is the area percentage of the four patterns of different indices

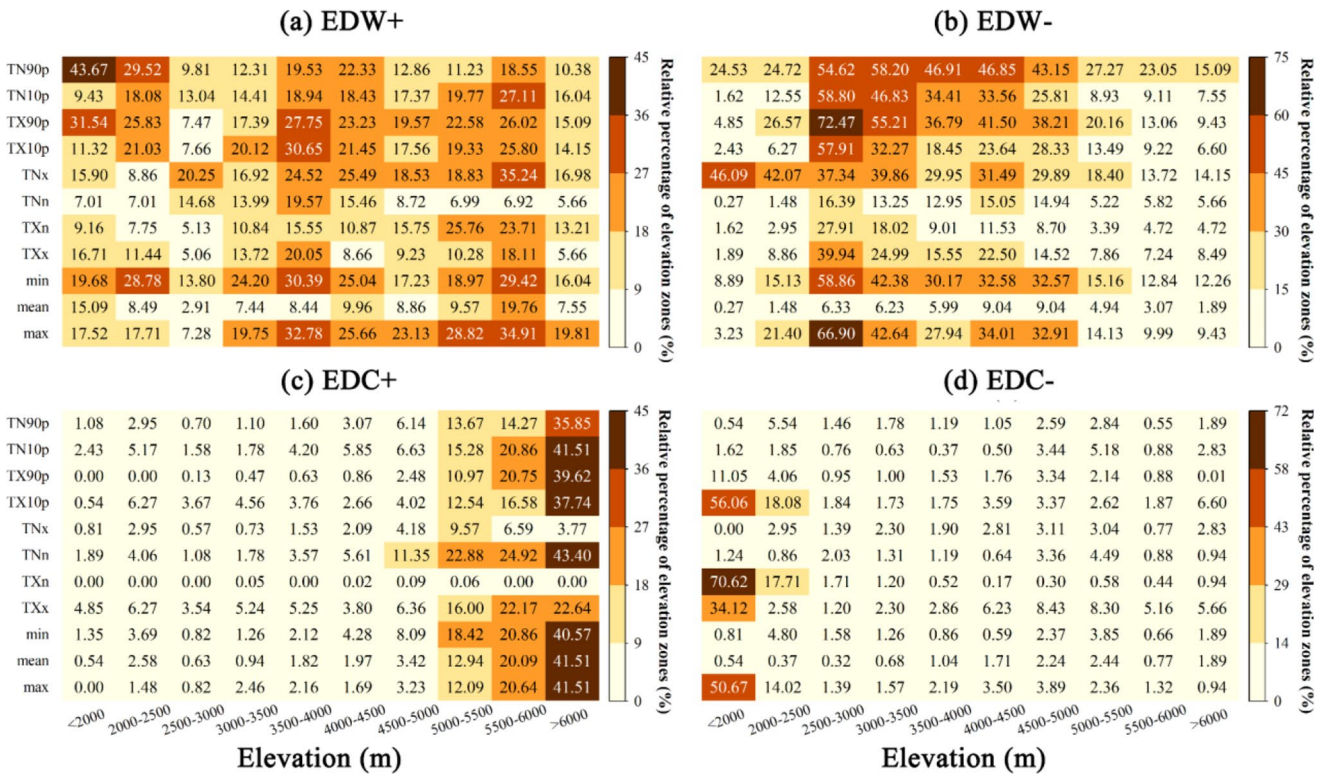

Fig. 4 Area percentage of each temperature elevation-dependent pattern at different elevation zones. The relative percentage is calculated by dividing the area of each temperature index at different elevation ranges by the total area of the TP at the corresponding elevation range

and the western of the Salween River basins at nighttime (Fig. 3m). Most of the EDW + signals occur at 3500–4500 m and 5000–6000 m while the EDW + of TX90p and TN90p is mainly below 2500 m (Fig. 4a).

EDW + has more severe impact on climate and ecosystems than EDW-. It also covers a relatively large area with average percentage of 35.91% in extreme temperature indices. Therefore, it is necessary to clarify the characteristics of extreme temperature warming with elevation. In the EDW + region, the magnitude of the increase in maximum temperature with elevation (0.17 °C/10a/km) is greater than that of the minimum (0.08 °C/10a/km) and mean (0.11 °C/10a/km) temperature. TXx (0.16 °C/10a/km) is larger than that of TNx (0.15 °C/10a/km), and TXn (0.30 °C/10a/km) is larger than that of TNn (0.14 °C/10a/km), indicating that the increase in daytime temperatures on TP is more closely related to elevation than nighttime. For the frequency of temperature extremes, warm days TX90p (2.56 d/10a/km) have a higher elevation dependency than warm nights TN90p (1.89 d/10a/km). Cold days TX10p (-2.74 d/10a/km) decrease faster with elevation than cold nights TN10p (-1.92 d/10a/km).

3.3 Attribution of temperature change patterns

Based on the theory that temperature changes with elevation is due to the elevation dependency of driving factors that can significantly affect temperature change, the driving factors must meet the following conditions: (1) They must significantly contribute to temperature changes even when the dependency on elevation is removed; (2) they must have elevation dependency (Yang et al. 2023; Rangwala et al. 2016). Atmospheric water vapor feedback, ice/snow albedo feedback, cloud feedback, and vegetation are considered important causes of elevation-dependent temperature change, as they directly or indirectly affect the surface energy balance (You et al. 2020a, b). Therefore, four variables are selected, including specific humidity, snow cover, total cloud cover, and NDVI (Fig. S3).

To satisfy the first condition, we calculate the trends of these variables (Fig. 5a-d) and remove the linear elevation dependency of these variables. Similarly, we also remove the linear elevation dependency of temperature change. After the adjustment, a significant correlation remains between the variables and temperature at the 0.05 significance level, with the average Pearson correlation coefficient r being 0.17, -0.04, -0.13 and −0.02 for specific humidity, total cloud cover, snow cover and NDVI, respectively. This indicates that, even after removing the elevation effect,

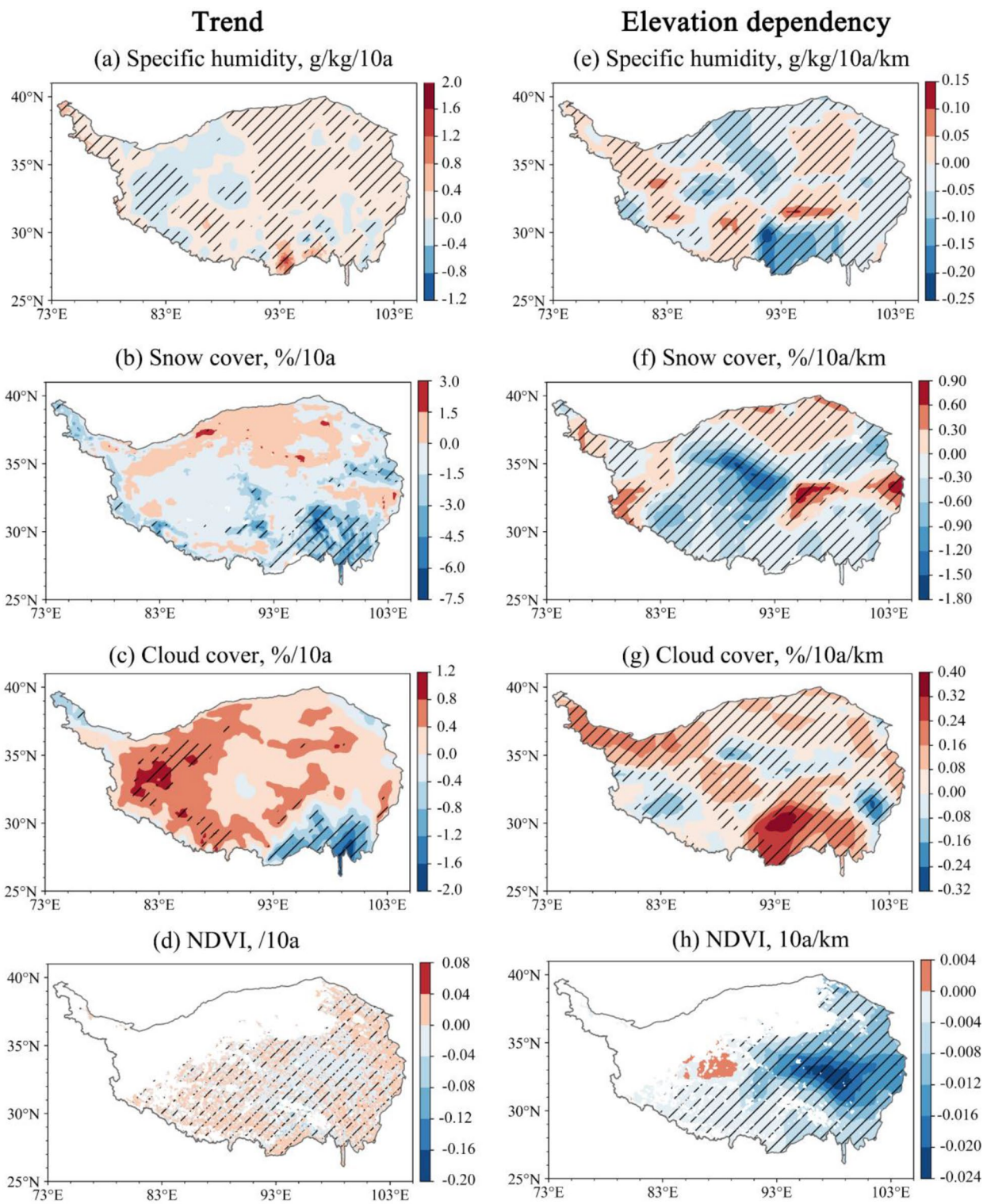

Fig. 5 Trends and elevation dependency of specific humidity, cloud cover, snow cover and NDVI. (**a**) - (**d**) are the trend of four variables. (**e**) - (**h**) are the elevation dependency of four variables. The shaded areas indicate correlations that are significant at the 0.05 level

the variables still have a significant impact on temperature change. Subsequently, the elevation dependency of these variables are calculated based on the original variable trend data (Fig. 5e-h). The GeoDetector model combined with a moving window is used to quantify the contribution of the elevation dependency of variable changes to the elevation dependency of temperature changes at each grid point. Specifically, each temperature index will generate four *q*-value maps, which correspond to the contribution of the elevation dependency of four driving factors to the elevation dependency of the temperature index. Given that the contribution of the same driving factor to each temperature indices is similar in space, we calculate the average spatial distribution of the *q*-value map for each driving factor (Fig. 6a-d). We focus on regions where EDW+/- and EDC+/- are centrally observed across all temperature indices (Fig. 3n). The mean *q*-values for distinct patterns of temperature changes (Fig. 6e) are therefore derived based on Fig. 3n. Additionally, the EDW+/- and EDC+/- regions referenced in the subsequent analysis are also based on Fig. 3n.

The attribution of four driving factors affecting temperature change patterns on the TP are spatially heterogeneous

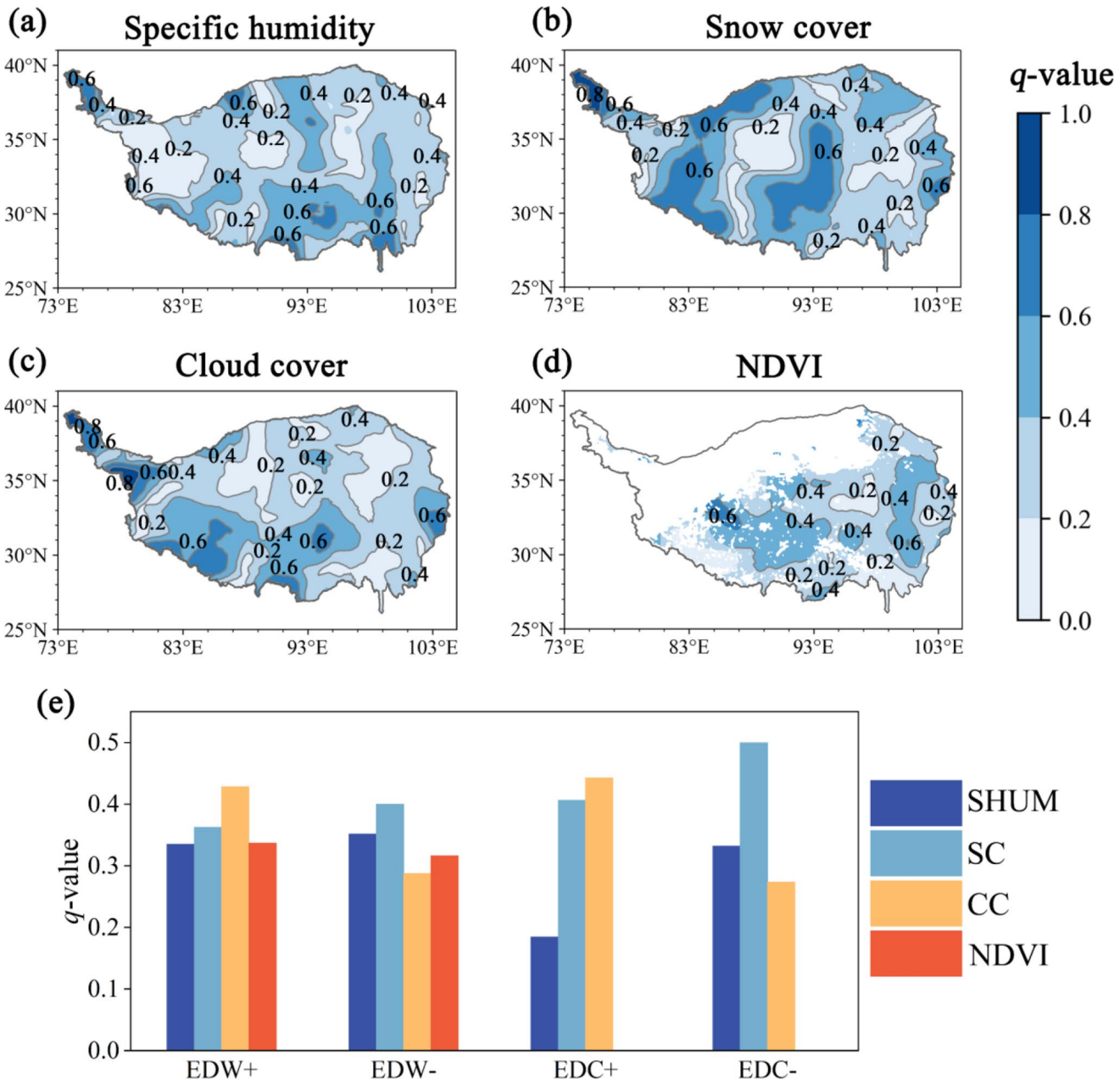

Fig. 6 The average contribution (*q*-value) of four driving factors. (**a**) – (**d**) are the spatial distribution of the mean *q*-value of 11 extreme temperature indices. (**e**) is the mean *q*-value of different patterns of temperature changes. SHUM: Specific humidity; SC: Snow cover; CC: Cloud cover

(Fig. 6a-d). The total cloud cover is the main cause of the elevation amplification effect of temperature change, including EDW+and EDC+with the highest *q*-values of 0.43 and 0.44, respectively (Fig. 6e). In EDW+region, the increase rate of the total cloud cover is 0.122%/10a, while the increase in total cloud cover is negative with elevation at the rate of -0.015%/10a/km (Table 2). It indicates that the increase in total cloud cover is smaller at higher elevations compared to lower elevations, allowing more shortwave radiation to be absorbed at higher elevations. This results in higher warming rates at high elevations than at low elevations, contributing to the formation of EDW+. In the EDW+region, the intensity and frequency of daytime temperature extremes are more related to elevation than at night. This phenomenon may be attributed to the dominant influence of shortwave radiation under the control of cloud. Compared to nighttime, high-elevation areas absorb more shortwave radiation during the daytime, resulting in a stronger elevation dependency. In the EDC+region, the total cloud cover is also increasing at the rate of 0.531%/10a, but it has a positive gradient with elevation at 0.106%/10a/km (Table 2). Therefore, in high-elevation areas, the increase in total cloud cover is greater than in low-elevation areas, resulting in less absorbed heat with increasing elevation, leading to the EDC+.

Snow cover is the primary driver of the elevation diminution effect on temperature change, including EDW- and EDC- with the highest *q*-values of 0.40 and 0.50 (Fig. 6e). In EDW- region, the snow is decreased at the rate of -0.357%/10a, and this decrease exhibits a positive gradient with elevation at the rate of 0.011%10a/km (Table 2). This leads to a slower decrease in surface albedo in high-elevation areas compared to low-elevation areas, resulting in a slower warming rate in high-elevation regions, thus forming EDW-. For EDC- region, the snow shows the opposite trend and elevation dependency to that in the EDW- region, which is 0.572%/10a and −0.355%/10a/km (Table 2). Increased snow cover increases the surface albedo, decreasing the temperature. Thus the negative rate of snow cover leads to the rate of cooling at higher elevations less than at lower elevations, forming the EDC-.

In addition, specific humidity contributes the most to the EDW- region with a *q*-value of 0.35 (Fig. 6e). Specific humidity is increasing at the rate of 0.116 g/kg/10a (Table 2). Increased atmospheric water vapor leads to enhanced downward longwave radiation, resulting in higher temperature. While its negative elevation dependency (-0.013 g/kg/10a/km) leads to higher warming at lower elevation than at higher elevation, contributing to the EDW- phenomenon. For NDVI, the overall vegetation trend in warming regions shows a decline at a rate of -0.003 /10a, suggesting that the cooling effect from vegetation plays a dominant role. It exhibits a negative elevation dependency with the rate of -0.005 10a/km on EDW+region. This means that, in lower-elevation areas, vegetation leads to a stronger cooling effect compared to higher-elevation areas. As a result, the warming amplitude at lower elevations is smaller than that at higher elevations, leading to the phenomenon of EDW+. Since EDC occurs at higher elevations where there is no vegetation (Fig. 4c and d), the contribution of vegetation is not included.

4 Discussion

4.1 Spatial heterogeneity and drivers of Elevation-dependent extreme temperature changes

In this study, the moving window model is applied for the first time to analyze the elevation dependency of temperature change on the TP. The model accurately provides a comprehensive and detailed spatial characterization of elevation dependency. The results show that there are four elevation-dependent patterns on the TP, including EDW+/- and

Table 2 Trend and elevation dependency of four driving factors

Type	Trend				Elevation dependency			
	SHUM (g/kg/10a)	SC (%/10a)	CC (%/10a)	NDVI (/10a)	SHUM (g/kg/10a/km)	SC (%/10a/km)	CC (%/10a/km)	NDVI (/10a/km)
EDW+	0.116	-1.132	0.122	-0.003	-0.013	-0.320	-0.015	-0.006
EDW-	0.116	-0.357	0.327	-0.003	-0.001	0.011	0.046	-0.005
EDC+	-0.007	-0.139	0.531	0	0.014	0.013	0.106	0
EDC-	-0.08	0.572	0.508	0	-0.026	-0.355	0.099	0

SHUM: specific humidity; SC: snow cover; CC: cloud cover. The main driving factors in different patterns are labeled

EDC+/- (Fig. 3). EDW+ is mainly concentrated in the southeastern TP, while EDW- is primarily found in the northern and central TP (Fig. 3n). The result resolves the contradictions in previous studies, where some reported EDW+ on TP (Hu and Hsu 2023), while others observed significant EDW- (Du et al. 2019). Additionally, we offer insights into the spatial distribution of EDC, which has been overlooked in other research. EDC+ mainly occurs in the northwestern TP, while EDC- is concentrated in the northern Inner TP (Fig. 3n). Previous studies treated the TP as a single entity, neglecting the spatial heterogeneity of temperature change patterns related to elevation. By employing the moving window model, we have achieved a more precise identification of EDW patterns across different regions of the TP.

The extreme temperature indices defined by the ETCCDI are included to investigate the elevation-dependent characteristics of extreme climate events. The results show that in EDW+ region, elevation dependency is more significant in maximum temperature trends (0.17 °C/10a/km) than in minimum temperature trends (0.08 °C/10a/km) (Fig. 3). However, some studies suggested that elevation dependency was more pronounced for minimum temperature trends (Sun et al. 2017, 2024; Yang et al. 2022). Wu et al. (2023) pointed out that ignoring the influence of latitude might lead to an underestimation of the elevation dependency of maximum temperature growth. The warming on TP is determined by the interaction between elevation and latitude, as warming in high-latitude regions typically rapid than that in low-latitude regions. By separating the effects of latitude and elevation on temperature change, they found that the impact of latitude on the increase in T_{max} is the most significant. As a result, when the latitude effect, which counteracts the elevation effect, is removed, the elevation dependency of T_{max} increases. In this study, after eliminating the effect of latitude using a moving window model, the maximum temperature changes have a closer relationship with elevation than minimum temperature changes. In addition, the increase in the intensity of extreme temperatures (0.16 °C/10a/km, 0.30 °C/10a/km, 0.15 °C/10a/km, 0.14 °C/10a/km for TXx, TXn, TNx and TNn) are more sensitive to elevation than the average state (0.11 °C/10a/km). Notably, the growth rate of TXn is approximately twice that of the other growth rates. This implies that the baseline for daytime maximum temperatures continues to rise. High-elevation regions are experiencing an increasing risk of extreme heat events, which will lead to significant snowmelt and permafrost degradation (Yang et al. 2019; Mu te al. 2020), resulting in a series of natural disasters such as landslides and floods (Tang et al. 2023). Additionally, higher temperatures may promote the upward migration of vegetation and advance the phenology of spring vegetation (Zhu et al. 2023), significantly affecting ecosystems.

In this study, the GeoDetector model combined with the moving window reveals the contributions of driving factors in different regions (Fig. 6). The dominant driving factor of the elevation amplification effect is the total cloud cover (q-value = 0.43 for EDW+ and q-value = 0.44 for EDC+). Total cloud cover is negatively correlated with temperature (Duan and Wu 2006). EDW+ primarily occurs between 3500 and 4500 m and 5000–6000 m (Fig. 4a), where the total cloud cover exhibits a negative elevation dependency (Fig. 5g). Consequently, higher elevations experience greater solar absorption and warming, as the growth rate of total cloud cover at these elevations is slower compared to lower elevations. Besides the total cloud cover, studies also revealed a significant upward shift of the snowline on the TP in recent years and emphasized its prominent contribution to EDW+ (You et al. 2020a, b). The upward shift of the snowline reduces albedo and accelerates the warming trend. Currently, the average snowline on the TP is around 5000 m (Zhang et al. 2022), so the EDW+ occurring between 5000 and 6000 m is not only attributed to the total cloud cover but also to the rising snowline. When the elevation exceeds 6000 m, the temperature no longer shows a warming trend, and the temperature change mode shifts to EDC+ (Fig. 4c). The positive elevation dependency of total cloud cover increase (Fig. 5g) results in less heat absorption at high elevations compared to low elevations, leading to the EDC+. Zhang et al. (2022) also pointed out that temperatures above 6000 m are primarily controlled by cloud cover. The reduction in cloud cover at high elevations leads to decreased heat absorption. Moreover, due to the stable snowpacks above 6000 m, a significant portion of the absorbed shortwave radiation is utilized for snowmelt rather than increasing air temperature, causing the temperature cooling rate to accelerate with increasing elevation.

The elevation diminution effect is mainly driven by snow cover (q-value = 0.40 for EDW- and q-value = 0.50 for EDC-). EDW- primarily occurs below the snowline, in the region between 2500 and 5000 m (Fig. 4b). In the EDW- region (Fig. 3n), decrease in snow cover exhibits a positive elevation dependency in most areas (Fig. 5f). At lower elevations, snow cover is more susceptible to change due to shallower snow depth. In contrast, higher elevations sustain relatively stable snow cover and snowline, resulting in prolonged snow persistence (Zhang et al. 2022). Consequently, snow cover retreats more rapidly at lower elevations than at higher elevations, leading to accelerated warming in lower-elevation regions. EDC- is primarily concentrated at elevations of 4500–5500 m (Fig. 4d), near the snowline. The heat generated by the upward shift of the snowline mitigates the preceding cooling trend, ultimately contributing to the formation of EDC-.

Models predict that temperatures on the TP will continue to rise in the coming decades (Chen et al. 2022), accompanied by reductions in both cloud cover (Yamamoto et al. 2024) and snow cover (Zou et al. 2022). These changes will lead to increased solar heat absorption at higher elevations, further intensifying the EDW+effect driven by cloud cover. If the rate of snowmelt at high elevations accelerates with rising temperatures and the snowline continues to move upward, the snow cover could shift to become a primary factor contributing to EDW+, posing a growing risk to the ecosystems of high-elevation areas and their downstream regions. In the future, patterns of elevation-dependent temperature change and changes in drivers need to be more accurately determined in order to minimise their deleterious effects.

4.2 Uncertainty analyses and implications

This paper reveals the elevation-dependent patterns of extreme temperature change and quantifies the contribution of the driving factors. The spatial air temperature data is the foundation of the study. Although the daily gridded air temperature data used in this study proved to be of high accuracy, the reliability of air temperatures in the northwestern TP and their relationship with elevation remains questionable due to the scarcity of station data in this region. Therefore, we first validate the reliability of the gridded data in areas with dense real temperature data based on 88 meteorological stations on TP. Since all extreme temperature indices are derived from T_{mean}, T_{max} and T_{min}, we only validate these three indices for the two datasets. The overall reliability of the temperature has been verified by Fang et al. (2022), but they overlooked the elevation-dependent biases. Therefore, we calculate the gradient of temperature changes with elevation for both gridded and station data. Then we analyze the consistency between the two datasets by linear regression. The results demonstrate a strong agreement between the gridded data and meteorological observations, with correlation coefficients r for T_{mean}, T_{min}, and T_{max} of 0.74 ($p<0.01$), 0.77 ($p<0.01$), and 0.74 ($p<0.01$), respectively, and corresponding RMSE values of 0.17 °C/100m, 0.18 °C/100m, and 0.16 °C/100m (Fig. 7b, Fig. S4a-b). A window with relatively dense stations shows the distribution of mean temperatures between the two datasets, indicating that the mean temperature in high-elevation areas is slightly underestimated compared to low-elevation areas (Fig. 7c). The mean temperature for each elevation band with 500 m is further calculated. The gridded data shows a slight systematic underestimation of the temperature (Fig. 7c and d). More importantly, this systematic underestimation is stable across the elevation band, which is not likely to have an impact on the elevation-dependent temperature changes. In general, although the meteorological stations are not evenly distributed within the window, which may influence the comparison, there is still a relatively high consistency between the station data and the gridded data. The verification results from the meteorological station data demonstrate the reliability of the gridded data. Additionally, in moving window applications, gridded data can effectively address issues such as uneven sample distribution across different windows.

Due to the inability to directly verify the accuracy of the dataset in the northwestern region, we use another dataset, China Meteorological Forcing Dataset (CMFD) (He et al. 2020), to validate the results of elevation dependency. There is high consistency in air temperature simulation, trends and elevation dependency calculations between two datasets, with r exceeding 0.74 (Table 3). The results also support the reliability of the data in this paper.

We focus on the annual extreme temperature changes, while previous studies had pointed out that elevation-dependent temperature changes exhibit significant seasonality, particularly with EDW+being more pronounced in winter and autumn (Wang et al. 2018). Meanwhile, the importance of driving factors in influencing elevation-dependent patterns varies across different seasons. Specifically, snow cover has a more important role in spring and summer due to its seasonal melting (Liu et al. 2009). The specific humidity is a key process in winter because the longwave radiation is more sensitive to moisture content at low humid levels (Ruckstuhl et al. 2007). For NDVI, the latent heat generated by vegetation and the changes in surface albedo differ between the growing and non-growing seasons, resulting in varying impacts on surface energy balance across different seasons (Wang et al. 2023). The contribution q-value of NDVI is relatively small (Fig. 6e), which may be attributed to the strong seasonality of vegetation. The annual average NDVI could diminish the ability of vegetation to influence elevation dependency.

In addition, only annual total cloud cover is used to quantify the cloud feedback effect on elevation dependency of temperature change, but cloud height and cloud amount can also play a significant role. Previous studies revealed that an increase in high cloud cover and a decrease in mid-level cloud cover lead to positive net cloud radiative forcing, which amplifies warming across much of the plateau (Hua et al. 2018). Furthermore, cloud cover has opposing effects on temperature during the daytime and nighttime. During the day, it primarily regulates shortwave radiation, whereas at night, it is more closely associated with longwave radiation. Extreme temperature indices also vary between day and night. Due to the lack of driving factors that differentiate between these periods, this paper uses the total cloud cover data and focuses on annual mean data to explain the

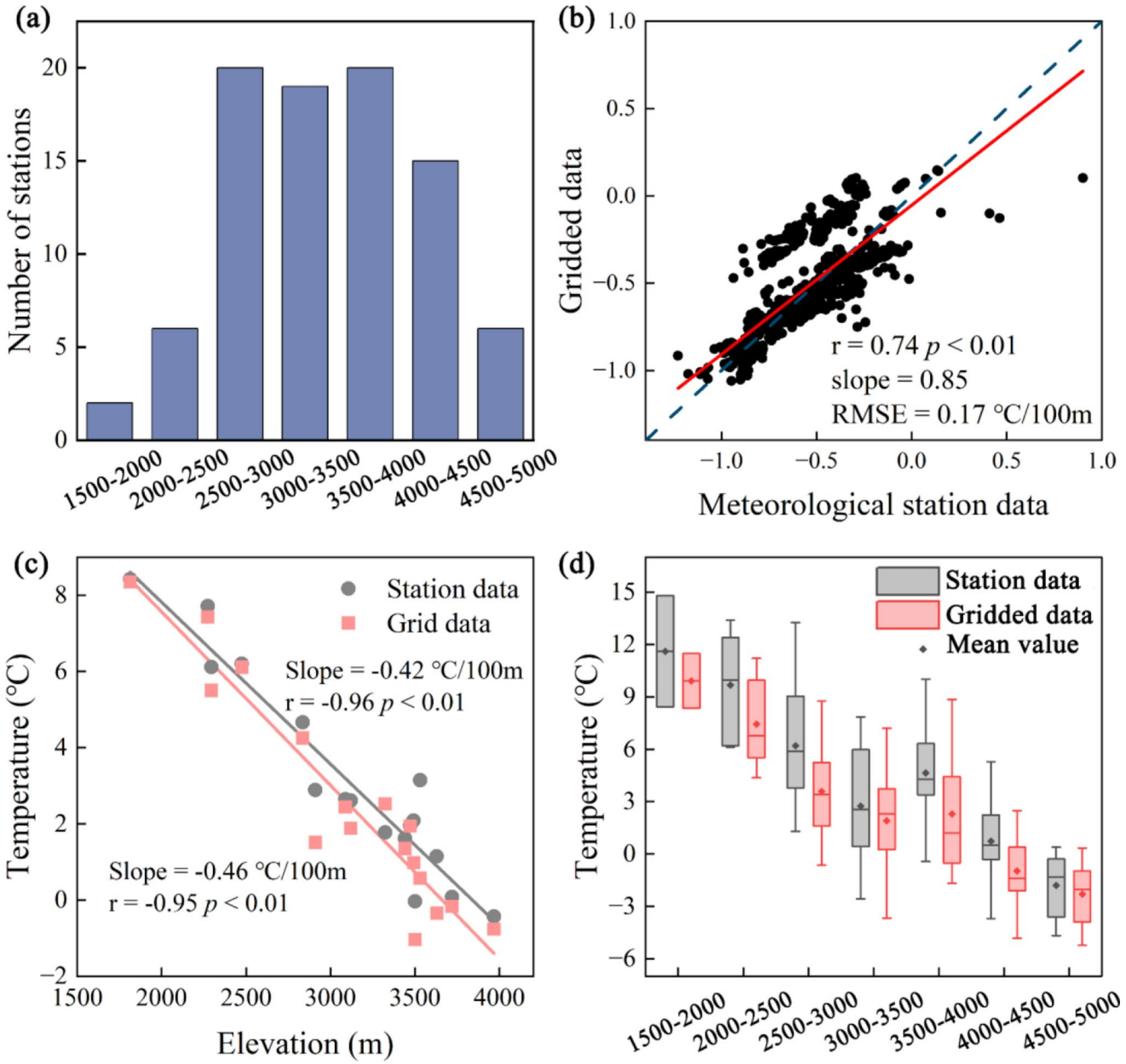

Fig. 7 Relationship between the meteorological stations data and gridded data for T_{mean}. (**a**) is the number of the meteorological stations at different elevation bands. (**b**) is the linear relationship for temperature gradient along elevation between t he meteorological stations data and gridded data. The dashed line is the 1:1 line. (**c**) is the relationship between the elevation and temperature for meteorological station data and gridded data at a certain window. (**d**) is the box plots of meteorological stations data and gridded data at different elevation bands. The diamond insides the box is the median value

Table 3 Correlation coefficients R and slope between daily gridded air temperature data used in this study and CMFD

	T_{max}		T_{mean}		T_{min}	
	r	Slope	*r*	Slope	*r*	Slope
Mean temperature	0.91	0.82	0.99	0.94	0.91	0.83
Trend	0.74	0.74	0.92	0.93	0.85	0.81
Elevation dependency	0.84	0.99	0.97	0.98	0.91	0.84

distribution and the mechanisms of different patterns of extreme temperature change. Therefore, future research needs to obtain more detailed driving factors data and focus on the seasonal changes of elevation-dependent temperature changes, aiming to reveal the more accurate contribution of its drivers.

5 Conclusions

This paper first applies the moving window model to identify the comprehensive spatial pattern of elevation dependency for extreme temperature change using the daily gridded air temperature data on TP from 1979 to 2018, and quantifies the contribution q-value of driving factors based on the GeoDetector model. The results show that there are four types of elevation-dependent patterns over the TP, including positive/negative elevation-dependent warming (EDW+/-, where warming trends strengthen/weaken with increasing elevation) and positive/negative elevation-dependent cooling (EDC+/-, where cooling trends strengthen/weaken with increasing elevation). EDW + is concentrated in southeast of TP and EDW- is in the north and center of TP. EDC + mainly occurs in the northeast of TP and EDC- is in the northern Inner TP. The total cloud cover is the main cause of the elevation amplification effect of extreme temperature change, with q-values of 0.43 and 0.44 for EDW + and EDC+, respectively. Its negative elevation dependency leads to more absorption of solar radiation at high elevations than at low elevations, thus creating EDW+. Conversely, the positive elevation dependency reduces the absorption of solar radiation and accelerates cooling at high elevations, leading to EDC+. Snow cover is the main cause of EDW- and EDC- with q-values of 0.40 and 0.50, respectively. Positive elevation dependency leads to reduced surface albedo and lower temperatures at high elevations, thus slowing warming, while negative elevation dependency leads to slower cooling at high elevations. This paper proposes a novel method for detecting spatial features of elevation dependency in extreme temperature change and provides vital insights into the temperature change pattern over the TP, which can certainly contribute to the understanding of the underlying mechanisms and potential impacts of climate change in alpine regions.

Supplementary Information The online version contains supplementary material available at https://doi.org/10.1007/s00382-025-07725-5.

Acknowledgements We thank the the National Tibetan Plateau Data Center, the European Centre for Medium-Range Weather Forecasts and the GIMMS team for providing the publicly available datasets.

Author contributions Ke Yang: Conceptualization, Formal analysis, Investigation, Methodology, Validation, Writing – original draft, Writing – review & editing. Weizhe Chen: Conceptualization, Funding acquisition, Methodology, Supervision, Writing – review & editing. Guoyu Ren: Writing – review & editing. Rui Zhang: Writing – review & editing.

Funding This study is supported by the National Natural Science Foundation of China (No. 42307556 and 42230208), the Natural Science Foundation of Hubei Province (No. 2023AFB024).

Data availability The daily gridded air temperature data (Fang et al. 2022) is available at https://zenodo.org/records/5502275.The ERA5 reanalysis data can be downloaded from https://www.ecmwf.int/en/forecasts/dataset/ecmwf-reanalysis-v5. The specific humidity data and another gridded air temperature dataset used to verify the reliability are derived from the China Meteorological Forcing Dataset (He et al. 2020) and can be available at https://doi.org/10.11888/AtmosphericPhysics.tpe.249369.file. The NDVI dataset from PKU GIMMS-NDVI product (Li et al. 2023) can be found at https://zenodo.org/records/8253971.

Declarations

Competing interests The authors declare that they have no known competing financial interests or personal relationships that could have appeared to influence the work reported in this paper.

References

Ahamed MRA, Maharana P, Dimri AP (2024) Elevation dependency of precipitation and temperature over Northeast India. Theor Appl Climatol 155:6409–6426

Che T, Hao XH, Dai LY, Li HY, Huang XD, Xiao L (2019) Snow cover variation and its impacts over the Qinghai-Tibet plateau. Bull Chin Acad Sci 34:1247–1253

Chen HP, Sun JQ (2015) Changes in climate extreme events in China associated with warming. Int J Climatol 35:2735–2751

Chen R, Li HY, Wang XJ, Gou XH, Yang MX, Wan GN (2022) Surface air temperature changes over the Tibetan plateau: historical evaluation and future projection based on CMIP6 models. Geosci Front 13:101452

Cuo L, Zhang YX, Wang QC, Zhang LL, Zhou BR, Hao ZC, Su FG (2013) Climate change on the Northern Tibetan plateau during 1957–2009: Spatial patterns and possible mechanisms. J Clim 26:85–109

Dimri AP, Palazzi E, Daloz AS (2022) Elevation dependent precipitation and temperature changes over Indian Himalayan region. Clim Dyn 59:1–21

Du MY, Liu JS, Li YN, Zhang FW, Zhao L, Niu B, He YT, Zhang XZ, Yonemura S, Tang YH (2019) Are high altitudinal regions warming faster than lower elevations on the Tibetan plateau?? Int J Glob Warm 18:363–384

Duan AM, Wu GX (2006) Change of cloud amount and the climate warming on the Tibetan plateau. Geophys Res Lett 33:1–5

Duan JP, Li L, Fang YJ (2015) Seasonal Spatial heterogeneity of warming rates on the Tibetan plateau over the past 30 years. Sci Rep 5:1–8

Fang S, Mao KB, Xia XQ, Wang P, Shi JC, Bateni SM, Xu TR, Cao MM, Heggy E, Qin ZH (2022) Dataset of daily near-surface air temperature in China from 1979 to 2018. Earth Syst Sci Data 14:1413–1432

Gao L, Deng HJ, Lei XY, Wei JH, Chen YN, Li ZQ, Ma MM, Chen XW, Chen Y, Liu MB, Gao JY (2021) Evidence of elevation-dependent warming from the Chinese Tian Shan. Cryosphere 15:5765–5783

Ghatak D, Sinsky E, Miller J (2014) Role of snow-albedo feedback in higher elevation warming over the Himalayas, Tibetan plateau and central Asia. Environ Res Lett 9:114008

Guo DL, Wang HJ (2012) The significant climate warming in the Northern Tibetan plateau and its possible causes. Int J Climatol 32:1775–1781

Guo DL, Sun JQ, Yang K, Pepin N, Xu YM (2019) Revisiting recent Elevation-Dependent warming on the Tibetan plateau using Satellite-Based data sets. J Geophys Res Atmos 124:8511–8521

Ha KJ, Yun KS (2012) Climate change effects on tropical night days in Seoul, Korea. Theor Appl Climatol 109:191–203

He J, Yang K, Tang WJ, Lu H, Qin J, Chen YY, Li X (2020) The first high-resolution meteorological forcing dataset for land process studies over China. Sci Data 7:1–11

Hu SZ, Hsu P-C (2023) Drivers of elevation-dependent warming over the Tibetan plateau. Atmos Ocean Sci Lett 16:100289

Hua S, Liu YZ, Jia R, Chang ST, Wu CQ, Zhu QZ, Shao TB, Wang B (2018) Role of clouds in accelerating cold-season warming during 2000–2015 over the Tibetan plateau. Int J Climatol 38:4950–4966

Huang JP, Zhou XJ, Wu GX, Xu XD, Zhao QY, Liu YM, Duan AM, Xie YK, Ma YM, Zhao P, Yang S, Yang K, Yang HJ, Bian JC, Fu YF, Ge JM, Liu YZ, Wu QG, Yu HP, Wang BB, Bao Q, Qie K (2023) Global climate impacts of Land-Surface and atmospheric processes over the Tibetan plateau. Rev Geophys 61:1–39

Ji BW, Qin YB, Zhang TB, Zhou XB, Yi GH, Zhang MT, Li ML (2022) Analyzing driving factors of drought in growing season in the inner Mongolia based on geodetector and GWR models. Remote Sens 14:6007

Kang SC, Xu YW, You QL, Flügel WA, Pepin N, Yao TD (2010) Review of climate and cryospheric change in the Tibetan plateau. Environ Res Lett 5:015101

Kang SC, Zhang QG, Qian Y, Ji ZM, Li CL, Cong ZY, Zhang YL, Guo JM, Du WT, Huang J, You QL, Panday AK, Rupakheti M, Chen DL, Gustafsson Ö, Thiemens MK, Qin DH (2019) Linking atmospheric pollution to cryospheric change in the third pole region: current progress and future prospects. Natl Sci Rev 6:796–809

Kjaersgaard JH, Cuenca RH, Martínez-Cob A, Gavilán P, Plauborg F, Mollerup M, Hansen S (2009) Comparison of the performance of net radiation calculation models. Theor Appl Climatol 98:57–66

Kuttippurath J, Patel VK, Sharma BR (2024) Observed changes in the climate and snow dynamics of the third pole. Npj Clim Atmos Sci 7:1–14

Lewis SC, King AD, Perkins-Kirkpkpatrick SE (2017) Defining a new normal for extremes in a warming world. Bull Am Meteorol Soc 98:1139–1152

Li CH, Su FG, Yang DQ, Tong K, Meng FC, Kan BY (2018) Spatiotemporal variation of snow cover over the Tibetan plateau based on MODIS snow product, 2001–2014. Int J Climatol 38:708–728

Li BF, Chen YN, Shi X (2020) Does elevation dependent warming exist in high mountain Asia? Environ Res Lett 15:024012

Li HX, Liu JR, Lei XL, Ju YM, Bu XX, Li HX (2022) Quantitative determination of environmental factors governing the snow melting: a geodetector case study in the central Tienshan mountains. Sci Rep 12:1–16

Li MY, Cao S, Zhu ZC, Wang Z, Myneni RB, Piao SL (2023) Spatiotemporally consistent global dataset of the GIMMS normalized difference vegetation index (PKU GIMMS NDVI) from 1982 to 2022. Earth Syst Sci Data 15:4877–4899

Liu XD, Chen BD (2000) Climatic warming in the Tibetan plateau during recent decades. Int J Climatol 20:1729–1742

Liu XD, Ping H (1998) Relationship between the Climatic warming over the Qinghai-Xizang plateau and its surrounding areas in recent 30 years and the elevation. Plateau Meteorol 17:245–249

Liu XD, Cheng ZG, Yan LB, Yin ZY (2009) Elevation dependency of recent and future minimum surface air temperature trends in the Tibetan plateau and its surroundings. Glob Planet Change 68:164–174

Liu LB, Wang Y, Wang Z, Li DL, Zhang YT, Qin DH (2019) Elevation-dependent decline in vegetation greening rate driven by increasing dryness based on three satellite NDVI datasets on the Tibetan plateau. Ecol Indic 107:105569

Liu J, Wu YM, Gao X (2021) Increase in occurrence of large glacier-related landslides in the high mountains of Asia. Sci Rep 11:1–12

Lu AG, Kang SC, Li ZX, Theakstone WH (2010) Altitude effects of Climatic variation on Tibetan plateau and its vicinities. J Earth Sci 21:189–198

Mazhar U, Jin SG, Duan WT, Bilal M, Ali MA, Farooq H (2021) Spatio-temporal trends of surface energy budget in Tibet from satellite remote sensing observations and reanalysis data. Remote Sens 13:1–20

Mu CC, Abbott BW, Norris AJ, Mu M, Fan CY, Chen X, Jia L, Yang RM, Zhang TJ, Wang K, Peng XQ, Wu QB, Guggenberger G, Wu XD (2020) The status and stability of permafrost carbon on the Tibetan plateau. Earth Sci Rev 211:103433

Pepin N, Bradley RS, Diaz HF, Baraer M, Caceres EB, Forsythe N, Fowler H, Greenwood G, Hashmi MZ, Liu XD, Miller JR, Ning L, Ohmura A, Palazzi E, Rangwala I, Schöner W, Severskiy I, Shahgedanova M, Wang MB, Williamson SN, Yang DQ (2015) Elevation-dependent warming in mountain regions of the world. Nat Clim Chang 5:424–430

Pepin N, Deng HJ, Zhang HB, Zhang F, Kang SC, Yao TD (2019) An examination of temperature trends at high elevations across the Tibetan plateau: the use of MODIS LST to understand patterns of Elevation-Dependent warming. J Geophys Res Atmos 124:5738–5756

Pepin NC, Arnone E, Gobiet A, Haslinger K, Kotlarski S, Notarnicola C, Palazzi E, Seibert P, Serafin S, Schöner W, Terzago S, Thornton JM, Vuille M, Adler C (2022) Climate changes and their elevational patterns in the mountains of the world. Rev Geophys 60:1–40

Post E, Steinman BA, Mann ME (2018) Acceleration of phenological advance and warming with latitude over the past century. Sci Rep 8:1–8

Qin YH, Liu WF, Guo ZH, Xue SB (2020) Spatial and Temporal variations in soil temperatures over the Qinghai – Tibet plateau from 1980 to 2017 based on reanalysis products. Theor Appl Climatol 140:1055–1069

Rangwala I, Miller JR (2012) Climate change in mountains: A review of elevation-dependent warming and its possible causes. Clim Change 114:527–547

Rangwala I, Sinsky E, Miller JR (2016) Variability in projected elevation dependent warming in boreal midlatitude winter in CMIP5 climate models and its potential drivers. Clim Dyn 46:2115–2122

Ruckstuhl C, Philipona R, Morland J, Ohmura A (2007) Observed relationship between surface specific humidity, integrated water vapor, and longwave downward radiation at different altitudes. J Geophys Res Atmos 112:1–7

Schoetter R, Cattiaux J, Douville H (2015) Changes of Western European heat wave characteristics projected by the CMIP5 ensemble. Clim Dyn 45:1601–1616

Shen MG, Piao SL, Jeong SJ, Zhou LM, Zeng ZZ, Ciais P, Chen DL, Huang MT, Jin CS, Li LZX, Li Y, Myneni RB, Yang K, Zhang GX, Zhang YJ, Yao TD (2015) Evaporative cooling over the Tibetan plateau induced by vegetation growth. Proc Natl Acad Sci U S A 112:9299–9304

Sun XB, Ren GY, Shrestha AB, Ren YY, You QL, Zhan YJ, Xu Y, Rupak R (2017) Changes in extreme temperature events over the Hindu Kush himalaya during 1961–2015. Adv Clim Chang Res 8:157–165

Sun Y, Hu T, Zhang XB (2024) Anthropogenic influence on altitudinally amplified temperature change in the Tibetan plateau. Environ Res Lett 19:1055–1069

Tang MG, Xu Q, Wang LN, Zhao HL, Wu GJ, Zhou J, Li G, Cai WJ, Chen X (2023) Hidden dangers of ice avalanches and glacier lake outburst floods on the Tibetan plateau: identification, inventory, and distribution. Landslides 20:2563–2581

Toledo O, Palazzi E, Cely Toro IM, Mortarini L (2022) Comparison of elevation-dependent warming and its drivers in the tropical and subtropical Andes. Clim Dyn 58:3057–3074

Wang JF, Zhang TL, Fu BJ (2016) A measure of Spatial stratified heterogeneity. Ecol Indic 67:250–256

Wang QQ, Wang MB, Fan XH (2018) Seasonal patterns of warming amplification of high-elevation stations across the Globe. Int J Climatol 38:3466–3473

Wang W, Samat A, Abuduwaili J, Ge YX (2021) Quantifying the influences of land surface parameters on LST variations based on geodetector model in Syr Darya basin, central Asia. J Arid Environ 186:104415

Wang QX, Fan XH, Wang MB (2022) Warming amplification with both altitude and latitude in the Tibetan plateau. Int J Climatol 42:3323–3340

Wang YB, You CH, Gao YH, Li YQ, Niu YY, Shao CL, Wang X, Xin XP, Yu GR, Han XG, Chen SP (2023) Seasonal variations and drivers of energy fluxes and partitioning along an aridity gradient in temperate grasslands of Northern China. Agric Meteorol 342:109736

Wei YQ, Fang YP (2013) Spatio-Temporal characteristics of global warming in the Tibetan plateau during the last 50 years based on a generalised temperature Zone - Elevation model. PLoS ONE 8:e60044

Wu FY, You QL, Cai ZY, Sun GD, Normatov I, Shrestha S (2023) Significant elevation dependent warming over the Tibetan plateau after removing longitude and latitude factors. Atmos Res 284:106603

Yamamoto ALC, Corrêa M, de Torres P, Martins RR, Godin-Beekmann FB S (2024) Total Ozone content, total cloud cover, and aerosol optical depth in CMIP6: simulations performance and projected changes. Theor Appl Climatol 155:2453–2471

Yan YP, You QL, Wu FY, Pepin N, Kang SC (2020) Surface mean temperature from the observational stations and multiple reanalyses over the Tibetan plateau. Clim Dyn 55:2405–2419

Yang K, Wu H, Qin J, Lin CG, Tang WJ, Chen YY (2014) Recent climate changes over the Tibetan plateau and their impacts on energy and water cycle: A review. Glob Planet Change 112:79–91

Yang MX, Wang XJ, Pang GJ, Wan GN, Liu ZC (2019) The Tibetan plateau cryosphere: observations and model simulations for current status and recent changes. Earth Sci Rev 190:353–369

Yang KK, Guo DL, Hua W, Pepin N, Yang K, Li D (2022) Tibetan plateau temperature extreme changes and their elevation dependency from Ground-Based observations. J Geophys Res Atmos 127:1–11

Yang Y, You QL, Zuo ZY, Zhang YQ, Liu Z, Kang SC, Zhai PM (2023) Elevation dependency of temperature trend over the Qinghai-Tibetan plateau during 1901–2015. Atmos Res 290:106791

Yao TD, Thompson LG, Mosbrugger V, Zhang F, Ma YM, Luo TX, Xu BQ, Yang XX, Joswiak DR, Wang WC, Joswiak ME, Devkota LP, Tayal S, Jilani R, Fayziev R (2012) Third pole environment (TPE). Environ Dev 3:52–64

Yao TD, Xue YK, Chen DL, Chen FH, Thompson L, Cui P, Koike T, Lau WKM, Lettenmaier D, Mosbrugger V, Zhang RH, Xu BQ, Dozier J, Gillespie T, Gu Y, Kang SC, Piao SL, Sugimoto S, Ueno K, Wang L, Wang WC, Zhang F, Sheng YW, Guo WD, Ailikun A, Yang XX, Ma YM, Shen SSP, Su ZB, Chen F, Liang SL, Liu YM, Singh VP, Yang K, Yang DQ, Zhao XQ, Qian Y, Zhang Y, Li Q (2019) Recent third Pole's rapid warming accompanies cryospheric melt and water cycle intensification and interactions between monsoon and environment: multidisciplinary approach with observations, modeling, and analysis. Bull Am Meteorol Soc 100:423–444

You QL, Kang SC, Aguilar E, Yan YP (2008) Changes in daily climate extremes in the Eastern and central Tibetan plateau during 1961–2005. J Geophys Res Atmos 113

You QL, Kang SC, Pepin N, Flügel WA, Yan YP, Behrawan H, Huang J (2010) Relationship between temperature trend magnitude, elevation and mean temperature in the Tibetan plateau from homogenized surface stations and reanalysis data. Glob Planet Change 71:124–133

You QL, Chen DL, Wu FY, Pepin N, Cai ZY, Ahrens B, Jiang ZH, Wu ZW, Kang SC, AghaKouchak A (2020a) Elevation dependent warming over the Tibetan plateau: patterns, mechanisms and perspectives. Earth Sci Rev 210:103349

You QL, Wu T, Shen LC, Pepin N, Zhang L, Jiang ZH, Wu ZW, Kang SC, AghaKouchak A (2020b) Review of snow cover variation over the Tibetan plateau and its influence on the broad climate system. Earth Sci Rev 201:103043

Yuan Z, Yin J, Wei MR, Yuan Y (2021) Spatio-temporal variations in the temperature and precipitation extremes in Yangtze river basin, China during 1961–2020. Atmos (Basel) 12:1–19

Zhang HB, Immerzeel WW, Zhang F, de Kok R, Chen DL, Yan W (2022) Snow cover persistence reverses the altitudinal patterns of warming above and below 5000 m on the Tibetan plateau. Sci Total Environ 803:149889

Zhu QA, Chen H, Peng CH, Liu JX, Piao SL, He JS, Wang SP, Zhao XQ, Zhang J, Fang XQ, Jin JX, Yang QE, Ren LL, Wang YF (2023) An early warning signal for grassland degradation on the Qinghai-Tibetan plateau. Nat Commun 14:6406

Zou H, Zhu JH, Zhou LB, Li P, Ma SP (2014) Validation and application of reanalysis temperature data over the Tibetan plateau. J Meteorol Res 28:139–149

Zou YF, Sun P, Ma ZC, Lv YF, Zhang Q (2022) Snow cover in the three stable snow cover areas of China and Spatio-Temporal patterns of the future. Remote Sens 14:3098

Terms and Conditions

Springer Nature journal content, brought to you courtesy of Springer Nature Customer Service Center GmbH (“Springer Nature”).
Springer Nature supports a reasonable amount of sharing of research papers by authors, subscribers and authorised users (“Users”), for small-scale personal, non-commercial use provided that all copyright, trade and service marks and other proprietary notices are maintained. By accessing, sharing, receiving or otherwise using the Springer Nature journal content you agree to these terms of use (“Terms”). For these purposes, Springer Nature considers academic use (by researchers and students) to be non-commercial.
These Terms are supplementary and will apply in addition to any applicable website terms and conditions, a relevant site licence or a personal subscription. These Terms will prevail over any conflict or ambiguity with regards to the relevant terms, a site licence or a personal subscription (to the extent of the conflict or ambiguity only). For Creative Commons-licensed articles, the terms of the Creative Commons license used will apply.
We collect and use personal data to provide access to the Springer Nature journal content. We may also use these personal data internally within ResearchGate and Springer Nature and as agreed share it, in an anonymised way, for purposes of tracking, analysis and reporting. We will not otherwise disclose your personal data outside the ResearchGate or the Springer Nature group of companies unless we have your permission as detailed in the Privacy Policy.
While Users may use the Springer Nature journal content for small scale, personal non-commercial use, it is important to note that Users may not:

1. use such content for the purpose of providing other users with access on a regular or large scale basis or as a means to circumvent access control;
2. use such content where to do so would be considered a criminal or statutory offence in any jurisdiction, or gives rise to civil liability, or is otherwise unlawful;
3. falsely or misleadingly imply or suggest endorsement, approval , sponsorship, or association unless explicitly agreed to by Springer Nature in writing;
4. use bots or other automated methods to access the content or redirect messages
5. override any security feature or exclusionary protocol; or
6. share the content in order to create substitute for Springer Nature products or services or a systematic database of Springer Nature journal content.

In line with the restriction against commercial use, Springer Nature does not permit the creation of a product or service that creates revenue, royalties, rent or income from our content or its inclusion as part of a paid for service or for other commercial gain. Springer Nature journal content cannot be used for inter-library loans and librarians may not upload Springer Nature journal content on a large scale into their, or any other, institutional repository.
These terms of use are reviewed regularly and may be amended at any time. Springer Nature is not obligated to publish any information or content on this website and may remove it or features or functionality at our sole discretion, at any time with or without notice. Springer Nature may revoke this licence to you at any time and remove access to any copies of the Springer Nature journal content which have been saved.
To the fullest extent permitted by law, Springer Nature makes no warranties, representations or guarantees to Users, either express or implied with respect to the Springer nature journal content and all parties disclaim and waive any implied warranties or warranties imposed by law, including merchantability or fitness for any particular purpose.
Please note that these rights do not automatically extend to content, data or other material published by Springer Nature that may be licensed from third parties.
If you would like to use or distribute our Springer Nature journal content to a wider audience or on a regular basis or in any other manner not expressly permitted by these Terms, please contact Springer Nature at

onlineservice@springernature.com